UNIVERSITY OF COPENHAGEN

Quantum Dot Parity Effects in Trivial and Topological Josephson Junctions

Razmadze, D.; O'Farrell, E. C. T.; Krogstrup, P.; Marcus, C. M.

Published in:
Physical Review Letters

DOI:
10.1103/PhysRevLett.125.116803

Publication date:
2020

Document version
Publisher's PDF, also known as Version of record

Citation for published version (APA):
Razmadze, D., O'Farrell, E. C. T., Krogstrup, P., & Marcus, C. M. (2020). Quantum Dot Parity Effects in Trivial and Topological Josephson Junctions. *Physical Review Letters*, *125*(11), [116803]. https://doi.org/10.1103/PhysRevLett.125.116803

Download date: 17. okt.. 2021

Quantum Dot Parity Effects in Trivial and Topological Josephson Junctions

D. Razmadze,[1,2] E. C. T. O'Farrell,[1,2] P. Krogstrup,[1,3] and C. M. Marcus[1,2]
[1]Center for Quantum Devices, Niels Bohr Institute, University of Copenhagen, 2100 Copenhagen, Denmark
[2]Microsoft Quantum Lab–Copenhagen, 2100 Copenhagen, Denmark
[3]Microsoft Quantum Materials Lab–Copenhagen, 2800 Kongens Lyngby, Denmark

(Received 24 May 2020; accepted 10 August 2020; published 8 September 2020)

An odd-occupied quantum dot in a Josephson junction can flip transmission phase, creating a π junction. When the junction couples topological superconductors, no phase flip is expected. We investigate this and related effects in a full-shell hybrid interferometer, using gate voltage to control dot-junction parity and axial magnetic flux to control the transition from trivial to topological superconductivity. Enhanced zero-bias conductance and critical current for odd parity in the topological phase reflects hybridization of the confined spin with zero-energy modes in the leads.

DOI: 10.1103/PhysRevLett.125.116803

The development of topologically protected qubits [1,2] for quantum computing [3,4] benefits from fundamental investigations that examine signatures of topological superconductivity in various device geometries. These serve both to test theoretical models and solidify the interpretation of experiments [5,6]. A fruitful system for exploring topological states is based on semiconductor nanowires with strong spin-orbit coupling in contact with a metallic superconductor [7–9]. Recently, semiconductor nanowires with a fully surrounding superconducting shell were found to offer a convenient means of tuning into the topological phase using applied axial magnetic flux [10]. In this system, the destructive Little-Parks effect [11], with the associated winding of the superconducting phase around the shell, induces a topological phase in the semiconductor core.

Here, we investigate Josephson junctions realized in full-shell InAs/Al nanowires, focusing on parity effects of a gate-controlled quantum dot in the junction. We investigate even and odd occupancies of the dot for the zeroth and first lobes of the reentrant Little-Parks structure in the leads. The hybrid nanowire containing the dot junction is embedded in a superconducting interferometer, allowing the phase across the dot junction to be measured relative to a reference arm containing a second gate-controlled junction. Depleting the reference junction *in situ* with a gate voltage allowed the dot junction to be measured in isolation, revealing related parity-dependent features in conductance.

Two main results are reported. First, differential conductance of the isolated dot junction as a function of applied voltage bias showed a strong zero-bias peak throughout the first lobe only for an odd-occupied dot junction, reminiscent of Kondo-enhanced zero-bias conductance peaks [12–14] seen for odd-occupied dots with superconducting leads [12–27]. To our knowledge, this effect has not been predicted or previously reported. When the dot junction had even occupancy, the zeroth and first superconducting lobes showed comparable conductance at all biases. Second, opening the interferometer, we observed a 0-π transition as a function of dot occupancy in the zero lobe, as previously reported [22,28–30], while in the first lobe, the 0-π transition was absent, as recently predicted [31–35] but not previously reported experimentally.

The absence of a π junction in the first lobe can be understood as resulting from hybridization (anticrossing) of the electronic level in the dot junction with zero-energy states in the leads, which protects the hybridized state around the junction from undergoing a parity switch where the corresponding unhybridized level would have crossed zero [35]. Hybridization of an odd junction state with *discrete* zero-energy states in the leads is reminiscent of, but distinct from, Kondo hybridization [36], which also favors a 0 junction [13,22,25,27,37,38].

Supercurrent through a conventional Josephson junction is given by $I = I_c \sin(\varphi)$, where I_c is the critical current and φ is the phase difference across the junction. In few-channel junctions, higher harmonics of $I(\varphi)$ are present, but the periodicity $I(\varphi) = I(\varphi + 2\pi)$ and symmetry $I(\varphi) = -I(-\varphi)$ remain [39]. Symmetry upon reversing phase can be lifted by spin-orbit fields [40,41], and a supercurrent at zero phase near a single-triplet anticrossing with topological leads was predicted [42]. Lifting of 2π periodicity by Majorana coupling [43,44] is not observed.

As discussed in recent proposals [31–35], the transmission phase through a quantum dot embedded in a Josephson junction—a well-studied system, see experimental [45] and theoretical [25,46] reviews—provides a means of investigating topological superconductivity. The Coulomb energy of the dot junction suppresses Cooper-pair tunneling, relying on spin-dependent cotunneling processes, which in turn depend on dot occupancy

 © 2020 American Physical Society

[27,28,30,47–50]. In its simplest form, for even dot parity (e state), the phase across the junction matches the conventional current-phase relation, while for odd parity (o state), supercurrent typically involves a sign reversal, $I = I_c \sin(\varphi + \pi) = -I_c \sin(\varphi)$, resulting in a supercurrent reversal or π junction.

InAs nanowires with ~130 nm diameter were grown by molecular beam epitaxy using the vapor-liquid-solid method, followed by *in situ* growth of a ~30 nm epitaxial Al shell fully surrounding the semiconductor core [51]. After placing the nanowires on an Si/SiO_2 substrate, polymer ramps were patterned to connect a loop and leads made of 25 nm of deposited Al, as shown in Fig. 1(c). The thin Al ensured that superconductivity was maintained in moderate fields along the nanowire axis. An insulating layer of HfO_2 (7 nm) was then deposited, followed by patterned Ti/Au top gates used to control electron density in regions where the Al was removed by wet etching. An electron micrograph of one of the devices is shown in Fig. 1(c), with false-colored active regions and uncolored gates set to +2 V. All wire segments exceed 1 μm, several times the Majorana localization length, $\xi \sim 180$ nm [10].

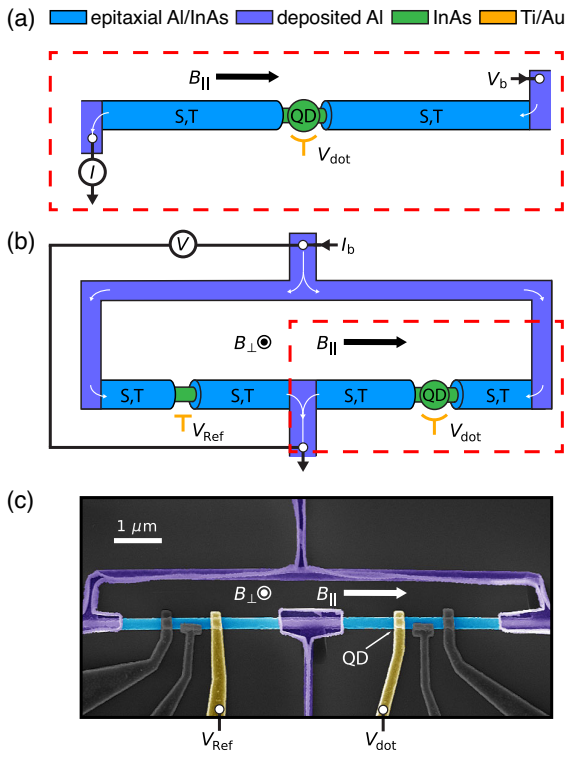

FIG. 1. (a) Schematic of a dot junction made from an InAs nanowire (green) containing a quantum dot (QD) with coupling and occupancy controlled by voltage V_{dot}. A voltage bias, V_b, with a small ac component was applied across the single dot junction and the current, I, measured. Thin Al leads (purple) remain superconducting with applied axial magnetic field $B_\parallel$. The lobe structure in the destructive Little-Parks regime accesses trivial (S) or topological (T) superconductivity in the leads [10]. (b) The dot junction was embedded in an interferometer with a reference junction controlled by gate voltage V_{Ref}. Current bias I_b with small ac component was applied and voltage V measured. Perpendicular field $B_\perp$ controlled interferometer phase. (c) False-color micrograph of a measured device showing a loop of thin Al deposited on ramps to contact the full-shell wire. Uncolored gates were set to +2 V.

Measurements were carried out in a dilution refrigerator with a base electron temperature of ~50 mK using conventional lock-in techniques in both voltage-bias and current-bias configurations. A vector magnet provided independent control of magnetic field along the wire axis $B_\parallel$, and a small transverse field $B_\perp$ was used to apply flux to the interferometer loop. A total of ten devices were cooled. Three devices were stable and showed similar behavior. One of those is presented in the main text and the other two in Figs. S1–S5 of the Supplemental Material (SM) [52]. Among the others, three were nonconducting or did not show a supercurrent, two showed excessive noise and did not have a controllable dot in the junction, one did not show a π junction in the zeroth lobe, and one appeared nontopological without a zero-bias feature in the first lobe and with π junction in both lobes. Differences in device behavior may reflect different wire diameters within the growth batch as well as disorder in the etched junction.

With the reference arm closed by setting $V_{Ref} = -2$ V, the dot junction was measured in a voltage-bias configuration, applying ac + dc voltage V_b (2 μV ac excitation) [see Fig. 1(a)]. At negative V_{dot}, approaching depletion, sharp resonances in tunneling conductance dI/dV_b were observed, indicating that a Coulomb blockaded quantum dot has formed in the junction. Note that V_{dot} controlled both the dot-junction occupancy and, on larger voltage scales, the coupling to the leads. Tunneling spectra at $B_\parallel = 0$, across a range of V_{dot} spanning two e states and one o state are shown in Fig. 2(a). A narrow supercurrent feature at zero bias can be seen throughout the sweep with two enhancements at the charge transition points, corresponding to Coulomb blockade resonances. Negative differential conductance in the zeroth lobe [green stripes in Fig. 2(a)] at low bias near the charge transitions and at higher bias in the e states presumably reflects the opening of weakly coupled channels that blockade transport [53]. The prevalence of these features in the e state indicates spin-dependent excited states for even occupancy.

Applying $B_\parallel$ reveals the lobe structure of destructive superconductivity, with suppressed superconductivity around $B_\parallel = 50$–60 mT and a first lobe centered around $B_\parallel = 120$ mT, corresponding to one quantum of applied flux and one twist of superconducting phase round the shell circumference. Figure 2(a) and 2(b) reveals a striking difference in bias spectra of the lobes. In particular, the first lobe [Fig. 2(b)] showed strongly enhanced zero-bias conductance in the o state but not in the e state, while spectra in the zeroth lobe showed similar conductance for both occupancies [Fig. 2(a)]. Bias spectra as a function of

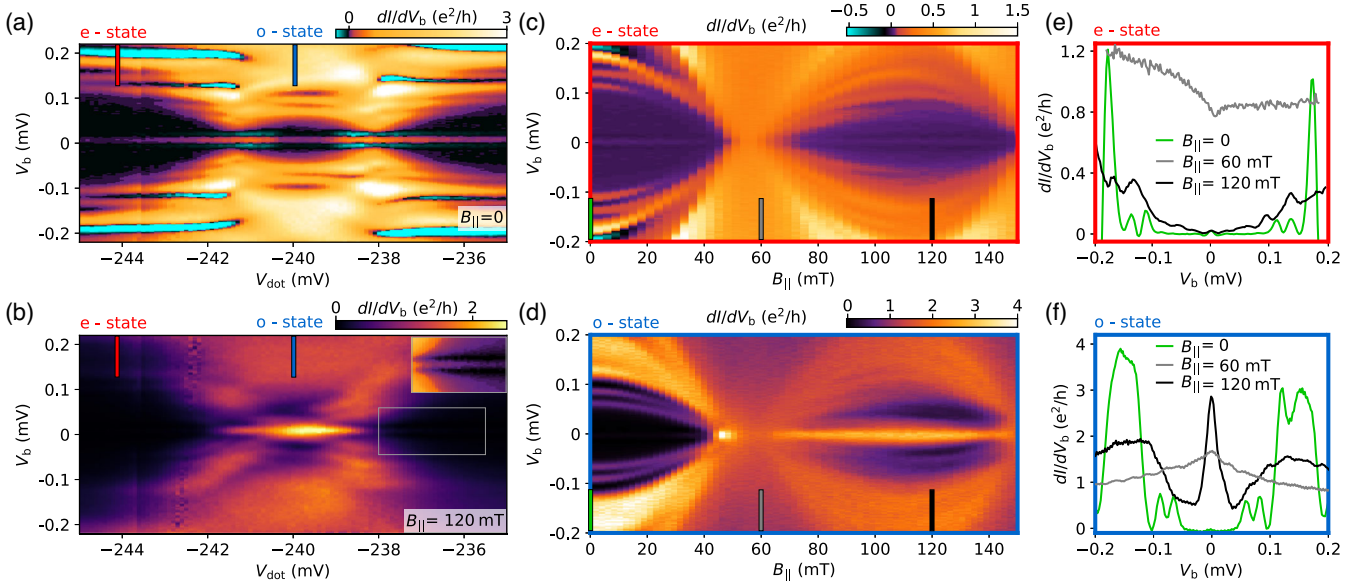

FIG. 2. Bias spectroscopy of the isolated dot junction with reference arm closed. (a) Differential conductance dI/dV_b as a function of gate voltage V_{dot} and dc bias V_b in the zero lobe ($B_{\|} = 0$). Sweeping V_{dot} changes dot occupancy from even (e state) to odd (o state) to even. A uniform conductance (supercurrent) peak at $V_b = 0$ is visible throughout the range of V_{dot}. Negative differential conductance features (green) are visible in the e state. Red (blue) marks indicate location of $e(o)$ state cuts in (c),(d). (b) Same as (a) except in the first lobe ($B_{\|} = 120$ mT). A strong enhancement of the zero-bias conductance peak occurs in the odd-occupied state. (c) Lobe structure in bias spectroscopy as a function $B_{\|}$ for e state. Green, gray, and black marks indicate cuts in (e). (d) Same as (c) for o state, with green, gray, and black marks indicating cuts in (f). Enhanced zero-bias conductance persists through the first lobe and does not split with increasing magnetic field. We interpret the isolated zero-bias peak at $B_{\|} \sim 46$ mT as a Kondo enhancement (see text). (e) Cuts from (c) in the e state showing small supercurrent peaks and several subgap resonances in both the zeroth (green) and first (black) lobes, with a broad zero-bias dip in the destructive regime (gray). (f) Cuts from (d) in the o state showing a large zero-bias conductance peak in the first lobe and a broad zero-bias peak in the destructive regime (gray).

$B_{\|}$ in Fig. 2(c) and 2(d) show a complementary view: In the zeroth lobe, o state and e state spectra are comparable, while throughout the first lobe the zero-bias conductance is strongly enhanced only for the o state, with enhancement roughly tracking the size of the topological gap. Cuts in Fig. 2(e) and 2(f) show a large zero-bias conductance peak in the first lobe for the o state, with 12 μV half-width at half maximum. Cuts along zero bias as a function of $B_{\|}$ are shown in Fig. S6 of the SM [52]. We note that the zero-bias peak in the o state in the first lobe does not appear to split with increasing $B_{\|}$. For a conventional Kondo peak in conductance, for instance arising from a soft gap in the first lobe [14], the peak would be split by $2g\mu_B B_{\|} > 50$ μeV in the first lobe, which would be visible.

We note in Fig. 2(d) a small, bright zero-bias peak at the closing of the zeroth lobe, $B_{\|} \sim 46$ mT. This small feature does not persist further into the zeroth lobe or into the destructive regime, where instead a broad zero-bias peak can be seen [gray cut in Fig. 2(f)], while in the e state, the destructive regime had a zero-bias dip [gray cut in Fig. 2(e)]. The bright peak at $B_{\|} \sim 46$ mT is more easily seen in the cut in Fig. S6 of the SM [52]. We interpret the narrow peak at $B_{\|} \sim 46$ mT as Kondo-enhanced conductance in the superconducting regime [12–14]. From the ratio of superconducting to normal conductance, $G_S/G_N \sim 2$, [from Figs. 2(d) and S6] we infer a rough ratio of Kondo temperature to gap, $T_K/\Delta \sim 2$ [12,13]. Within this interpretation, the width of the peak and its appearance only at the closing of the zero lobe suggests a low T_K of order 10 μeV. The zero-bias peak in the o state destructive regime presumably reflects normal-state Kondo enhancement.

Opening the reference arm by setting $V_{\mathrm{Ref}} = 0$ V connected the interferometer loop, yielding a switching current of 2 nA in the reference junction compared to ~1 nA in the dot junction. In the configuration of Fig. 1(b), whenever the current bias I_b exceeded the total switching current of the interferometer, a finite differential resistance, dV/dI_b, appeared across the interferometer. Figure 3(a) shows dV/dI_b for dc current bias $I_b = 2$ nA (with ac excitation 0.2 nA) as a function of V_{dot} and $B_{\perp}$ in the zeroth lobe, with $B_{\|} = 0$. To avoid hysteretic effects, I_b was briefly set to zero then reset to 2 nA for each data point (pixel) in the two-dimensional plot. Figure 3(a) shows the periodic dependence of the zero-resistance state with magnetic flux through the interferometer, consistent with $\Delta B_{\perp} A = \Phi_0 = h/2e$, where A is the interferometer area. As V_{dot} was swept from the e state to the o state, the phase of oscillation with $B_{\perp}$ shifted by $\Phi_0/2$, indicating that the dot junction is a π junction in the o state relative to the e state.

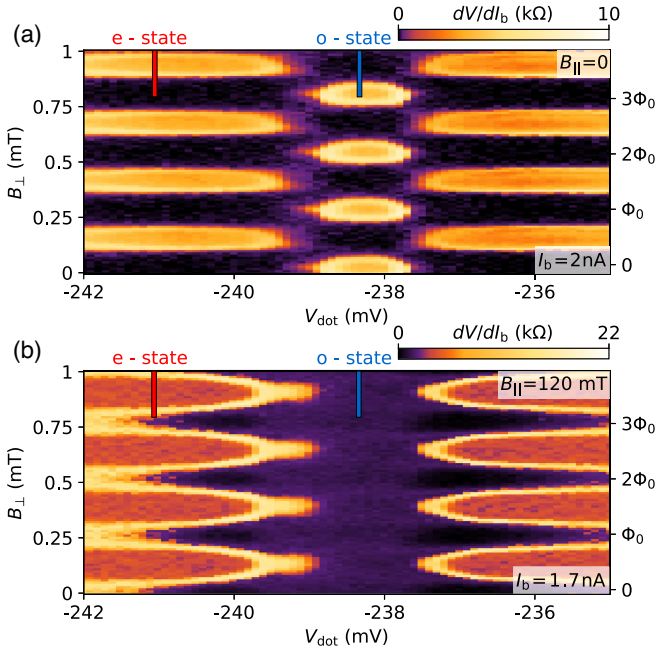

FIG. 3. Differential resistance dV/dI_b of the interferometer as a function gate voltage V_{dot} controlling dot occupancy and $B_\perp$ controlling flux through the interferometer. Current bias I_b was set to periodically exceed the total switching current of the interferometer. (a) The zeroth lobe ($B_\parallel = 0$) with $I_b = 2$ nA showed a π phase shift in the o state relative to the e state, indicating a π junction. (b) Same as (a) except in the first lobe ($B_\parallel = 120$ mT) with $I_b = 1.7$ nA, showing no phase shift as a function of V_{dot}.

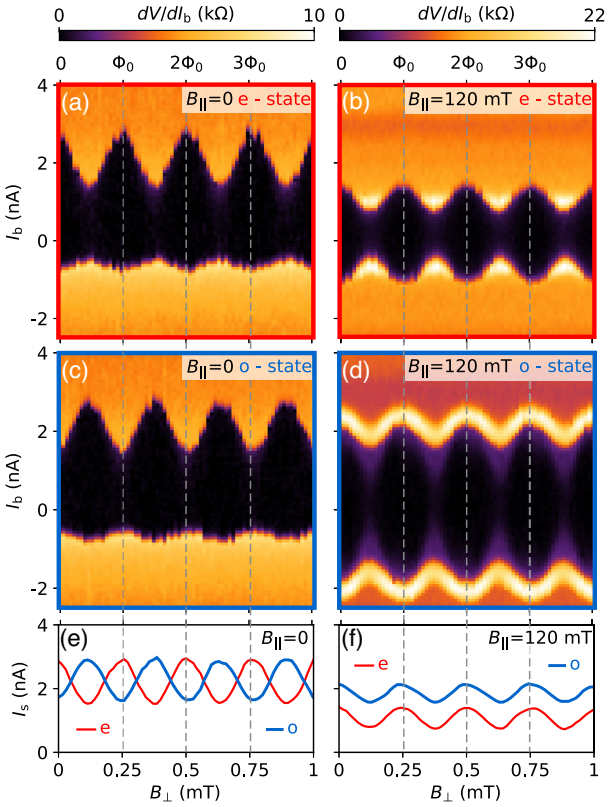

FIG. 4. Differential resistance dV/dI_b of the interferometer as a function of bias current I_b and perpendicular magnetic field $B_\perp$, (a),(c) in the zeroth lobe, along cuts through the $e(o)$ state [red (blue) marks in Fig. 3(a)], showing relative π phase shift, and (b), (d) in the first lobe, along cuts through the $e(o)$ state [red (blue) marks in Fig. 3(b)], showing absence of phase shift. Note in (a), (c) that switching currents exceed retrapping currents. (b),(d) In the first lobe ($B_\parallel = 120$ mT), switching and retrapping currents are comparable. (e) Relative phase shift of π between e state (red) and o state (blue) in the zeroth lobe. (f) No phase shift between the e state (red) and o state (blue) in the first lobe ($B_\parallel = 0$), where both phases align with the e state (red) in the zeroth lobe. Critical current in the o state (blue) exceeds the e state (red) in the first lobe ($B_\parallel = 120$ mT).

Figure 3(b) shows a similar plot, now in the first lobe ($B_\parallel = 120$ mT), demonstrating the *absence* of a π phase shift for relative occupancies. The absence of π-junction behavior for topological dot junctions is consistent with theoretical predictions [33–35]. Oscillations in dV/dI_b are less visible in the o state in the first lobe [Fig. 3(b)] compared to the zeroth lobe [Fig. 3(a)], as the switching current of the dot junction was larger in the o state in first lobe, barely exceeding the bias $I_b = 2$ nA. This is more clearly seen by measuring dV/dI_b as function of a swept I_b, as shown in Fig. 4. Differential resistance dV/dI_b of the interferometer along cuts through the e state and o state of the dot junction showed oscillatory patterns of switching and retrapping currents with applied flux, noting that I_b was stepped from negative to positive. Similar data for the other devices are shown in Figs. S4 and S6 of the SM [52]. Phase plots at other fields for device 1 are shown in Fig. S7 of the SM [52].

We draw attention to several features in Fig. 4: (i) There is a π phase shift between panels (a) and (c), indicating that in the zeroth lobe, the o state forms a π junction relative to the e state. (ii) There is no π phase shift between panels (b) and (d), indicating that in the first lobe there is no relative π junction upon changing dot occupancy. We do not observe a nontrivial phase shift in (d), noting that $B_\parallel$ is probably too small to induce a single-triplet crossing [42]. (iii) The absolute phase is the same in all four panels, with only the o state in the zeroth lobe shifted by π [panel (c)]. Phase was not corrected for a given $B_\parallel$. (iv) Retrapping currents are smaller than switching currents the zeroth lobe [panels (a,c)] but are comparable in the first lobe, presumably due to subgap modes that both dampen junction dynamics and cool the junction through the leads. (v) Switching and retrapping currents in the e state and the o state are comparable in the zeroth lobe [panels (a),(c), (e)], whereas in the first lobe, switching currents are larger in the o state than in the e state [see panels (b),(d),(f)]. As with the enhanced first-lobe conductance in the o state (Fig. 2), this observation is not anticipated theoretically. Dependencies of critical current on gate voltage, also

showing enhanced critical current in the first lobe for the o state, are shown in Fig. S9 of the SM [52].

Finally, we revisit the feature at $B_{\parallel} \sim 46$ mT, interpreted above as Kondo-enhanced conductance as the first lobe closes, in the interferometer configuration. Enhanced critical current, $I_c \sim 1$ nA, and 0-junction behavior at that location—contrasting the π-junction behavior within the zeroth lobe (Fig. S8 in the SM [52])—is consistent with an estimate for an overdamped junction, $G_S/G_N \sim \exp(\hbar I_c/ek_BT)$ [13]. Taking $G_S/G_N \sim 2$ and $T \sim 50$ mK yields $I_c \sim 1$ nA, close to the measured value.

We thank A. Akhmerov, K. Flensberg, L. Fu, L. Glazman, J. Paaske, C. Schrade, J. Schulenborg, G. Steffensen, and S. Vaitiekėnas for valuable discussions, and S. Upadhyay for help with fabrication. Research is supported by Microsoft, the Danish National Research Foundation, and the European Research Commission, Grant No. 716655.

[1] J. Alicea, Y. Oreg, G. Refael, F. von Oppen, and M. P. A. Fisher, Nat. Phys. **7**, 412 (2011).
[2] D. Aasen, M. Hell, R. V. Mishmash, A. Higginbotham, J. Danon, M. Leijnse, T. S. Jespersen, J. A. Folk, C. M. Marcus, K. Flensberg, and J. Alicea, Phys. Rev. X **6**, 031016 (2016).
[3] A. Y. Kitaev, Ann. Phys. (Amsterdam) **303**, 2 (2003).
[4] C. Nayak, S. H. Simon, A. Stern, M. Freedman, and S. Das Sarma, Rev. Mod. Phys. **80**, 1083 (2008).
[5] P. San-Jose, J. Cayao, E. Prada, and R. Aguado, Sci. Rep. **6**, 21427 (2016).
[6] J. Cayao, E. Prada, P. San-Jose, and R. Aguado, Phys. Rev. B **91**, 024514 (2015).
[7] Y. Oreg, G. Refael, and F. von Oppen, Phys. Rev. Lett. **105**, 177002 (2010).
[8] R. M. Lutchyn, J. D. Sau, and S. Das Sarma, Phys. Rev. Lett. **105**, 077001 (2010).
[9] R. M. Lutchyn, E. P. A. M. Bakkers, L. P. Kouwenhoven, P. Krogstrup, C. M. Marcus, and Y. Oreg, Nat. Rev. Mater. **3**, 52 (2018).
[10] S. Vaitiekėnas, G. W. Winkler, B. van Heck, T. Karzig, M.-T. Deng, K. Flensberg, L. I. Glazman, C. Nayak, P. Krogstrup, R. M. Lutchyn, and C. M. Marcus, Science **367**, eaav3392 (2020).
[11] W. A. Little and R. D. Parks, Phys. Rev. Lett. **9**, 9 (1962).
[12] M. R. Buitelaar, T. Nussbaumer, and C. Schönenberger, Phys. Rev. Lett. **89**, 256801 (2002).
[13] M.-S. Choi, M. Lee, K. Kang, and W. Belzig, Phys. Rev. B **70**, 020502(R) (2004).
[14] E. J. H. Lee, X. Jiang, R. Aguado, G. Katsaros, C. M. Lieber, and S. De Franceschi, Phys. Rev. Lett. **109**, 186802 (2012).
[15] K. Grove-Rasmussen, H. I. Jørgensen, and P. E. Lindelof, New J. Phys. **9**, 124 (2007).
[16] T. Sand-Jespersen, J. Paaske, B. M. Andersen, K. Grove-Rasmussen, H. I. Jørgensen, M. Aagesen, C. B. Sørensen, P. E. Lindelof, K. Flensberg, and J. Nygård, Phys. Rev. Lett. **99**, 126603 (2007).
[17] A. Eichler, M. Weiss, S. Oberholzer, C. Schönenberger, A. Levy Yeyati, J. C. Cuevas, and A. Martín-Rodero, Phys. Rev. Lett. **99**, 126602 (2007).
[18] C. Buizert, A. Oiwa, K. Shibata, K. Hirakawa, and S. Tarucha, Phys. Rev. Lett. **99**, 136806 (2007).
[19] C. Karrasch, A. Oguri, and V. Meden, Phys. Rev. B **77**, 024517 (2008).
[20] A. Eichler, R. Deblock, M. Weiss, C. Karrasch, V. Meden, C. Schönenberger, and H. Bouchiat, Phys. Rev. B **79**, 161407(R) (2009).
[21] Y. Kanai, R. S. Deacon, A. Oiwa, K. Yoshida, K. Shibata, K. Hirakawa, and S. Tarucha, Phys. Rev. B **82**, 054512 (2010).
[22] R. Maurand, T. Meng, E. Bonet, S. Florens, L. Marty, and W. Wernsdorfer, Phys. Rev. X **2**, 011009 (2012).
[23] W. Chang, V. E. Manucharyan, T. S. Jespersen, J. Nygård, and C. M. Marcus, Phys. Rev. Lett. **110**, 217005 (2013).
[24] R. Žitko, J. S. Lim, R. López, and R. Aguado, Phys. Rev. B **91**, 045441 (2015).
[25] V. Meden, J. Phys. Condens. Matter **31**, 163001 (2019).
[26] J. C. Estrada Saldaña, R. Žitko, J. P. Cleuziou, E. J. H. Lee, V. Zannier, D. Ercolani, L. Sorba, R. Aguado, and S. De Franceschi, Sci. Adv. **5**, eaav1235 (2019).
[27] A. Kadlecová, M. Žonda, V. Pokorný, and T. Novotný, Phys. Rev. Applied **11**, 044094 (2019).
[28] J. A. van Dam, Y. V. Nazarov, E. P. A. M. Bakkers, S. De Franceschi, and L. P. Kouwenhoven, Nature (London) **442**, 667 (2006).
[29] H. I. Jørgensen, T. Novotný, K. Grove-Rasmussen, K. Flensberg, and P. E. Lindelof, Nano Lett. **7**, 2441 (2007).
[30] R. Delagrange, R. Weil, A. Kasumov, M. Ferrier, H. Bouchiat, and R. Deblock, Phys. Rev. B **93**, 195437 (2016).
[31] Z. Gao, W. J. Gong, S. F. Zhang, G. Y. Yi, and Y. S. Zheng, Europhys. Lett. **109**, 40010 (2015).
[32] A. Camjayi, L. Arrachea, A. Aligia, and F. von Oppen, Phys. Rev. Lett. **119**, 046801 (2017).
[33] C. Schrade and L. Fu, arXiv:1809.06370.
[34] O. A. Awoga, J. Cayao, and A. M. Black-Schaffer, Phys. Rev. Lett. **123**, 117001 (2019).
[35] J. Schulenborg and K. Flensberg, Phys. Rev. B **101**, 014512 (2020).
[36] M. Cheng, M. Becker, B. Bauer, and R. M. Lutchyn, Phys. Rev. X **4**, 031051 (2014).
[37] G. Sellier, T. Kopp, J. Kroha, and Y. S. Barash, Phys. Rev. B **72**, 174502 (2005).
[38] R. Allub and C. R. Proetto, Phys. Rev. B **91**, 045442 (2015).
[39] E. M. Spanton, M. T. Deng, S. Vaitiekėnas, P. Krogstrup, J. Nygård, C. M. Marcus, and K. A. Moler, Nat. Phys. **13**, 1177 (2017).
[40] A. Zazunov, R. Egger, T. Jonckheere, and T. Martin, Phys. Rev. Lett. **103**, 147004 (2009).
[41] D. B. Szombati, S. Nadj-Perge, D. Car, S. R. Plissard, E. P. A. M. Bakkers, and L. P. Kouwenhoven, Nat. Phys. **12**, 568 (2016).
[42] C. Schrade, S. Hoffman, and D. Loss, Phys. Rev. B **95**, 195421 (2017).
[43] L. Fu and C. L. Kane, Phys. Rev. B **79**, 161408(R) (2009).
[44] M. Veldhorst, C. G. Molenaar, C. J. M. Verwijs, H. Hilgenkamp, and A. Brinkman, Phys. Rev. B **86**, 024509 (2012).

[45] S. De Franceschi, L. Kouwenhoven, C. Schönenberger, and W. Wernsdorfer, Nat. Nanotechnol. **5**, 703 (2010).
[46] A. Martín-Rodero and A. Levy Yeyati, Adv. Phys. **60**, 899 (2011).
[47] L. Glazman and K. Matveev, JETP Lett. **49**, 659 (1989), https://ui.adsabs.harvard.edu/abs/1989JETPL..49..659G.
[48] B. I. Spivak and S. A. Kivelson, Phys. Rev. B **43**, 3740 (1991).
[49] A. V. Rozhkov, D. P. Arovas, and F. Guinea, Phys. Rev. B **64**, 233301 (2001).
[50] E. Vecino, A. Martín-Rodero, and A. Levy Yeyati, Phys. Rev. B **68**, 035105 (2003).
[51] P. Krogstrup, N. L. B. Ziino, W. Chang, S. M. Albrecht, M. H. Madsen, E. Johnson, J. Nygård, C. M. Marcus, and T. S. Jespersen, Nat. Mater. **14**, 400 (2015).
[52] See Supplemental Material at http://link.aps.org/supplemental/10.1103/PhysRevLett.125.116803 for data from other devices and additional data for device 1.
[53] F. W. J. Hekking, L. I. Glazman, K. A. Matveev, and R. I. Shekhter, Phys. Rev. Lett. **70**, 4138 (1993).